CHEMICALLY-SELECTIVE 3D MRI OF LABORATORY OIL-WATER DISPLACEMENT PROCESSES

N.P. Ramskill[a*], I. Bush[a], A.J. Sederman[a], M.D. Mantle[a], B.C. Anger[b], M. Appel[b], L.F. Gladden[a]

[a] Department of Chemical Engineering and Biotechnology, University of Cambridge, Cambridge CB2 3RA, UK.
[b] Shell Technology Centre, 3333 Highway 6 S, Houston, Texas, U.S.A.

This paper was prepared for presentation at the International Symposium of the Society of Core Analysts held in Snowmass, Colorado, USA, 21-26 August 2016

ABSTRACT

Successful deployment of improved oil recovery (IOR) and enhanced oil recovery (EOR) technology in the field relies on the correct interpretation of laboratory core analysis data. In systems that exhibit heterogeneous fluid distributions within the rock during a core flood, for instance due to the capillary end effect or viscous fingering, 3D visualization is required to fully characterise the relatively complex displacement mechanisms associated with such cases. Furthermore, it is desirable to monitor the different phases present in the rock sample *directly* without the addition of dopants that can potentially alter the fluid-rock surface interaction. In this work, we have demonstrated the implementation of a magnetic resonance imaging (MRI) technique to provide high-temporal resolution, chemically-specific 3D images of hydrocarbon and aqueous phases within a rock core during a core flood. We have previously shown that by using the rapid acquisition with relaxation enhancement (RARE) pulse sequence combined with Compressed Sensing (CS), it is possible to reconstruct a near-perfect image from significantly fewer measurements than would be necessary using conventional acquisition strategies, and this can result in significant reductions in the image acquisition times. In the present work, the CS-RARE approach has been extended to include chemically-selective excitations which have enabled independent 3D images of the oil and water distributions within the rock core to be obtained. To demonstrate the application of this technique, the drainage of dodecane into a water-saturated Estaillades limestone core plug has been investigated. The 3D images of the oil and water saturations can provide new insight into the dynamics of the displacement mechanisms taking place.

INTRODUCTION

Laboratory-scale displacements in rock core-plug samples (core floods) are widely used to develop understanding of the displacement mechanisms occurring during improved oil recovery (IOR) and enhanced oil recovery (EOR) processes [1]. In systems that exhibit heterogeneous fluid distributions within the rock during a core flood, for instance due to the capillary end effect [2] or viscous fingering [3], 3D visualization of the hydrocarbon and aqueous phases is required to fully characterise the relatively complex displacement mechanisms associated with such cases.

Nuclear magnetic resonance (NMR) and magnetic resonance imaging (MRI) have been used extensively in a range of areas within special core analysis and petrophysics research. For instance, NMR relaxometry and diffusometry have been used for structural characterisation of core plugs [4], quantification of oil and water content during laboratory core floods [5], measurement of fluid properties [6] and probing core plug wettabilities [7]. MRI techniques have previously been used for mapping heterogeneities within core plug samples [8], monitoring fluid distributions [9] and flow fields [10] during laboratory core floods. However, the acquisition times for high spatial resolution 3D images using traditional MRI techniques, such as spin-warp [11], are typically too long to capture the dynamic nature of the displacement mechanisms that are of interest.

Reductions in the acquisition times of the imaging experiment can be achieved using ultra-fast MRI pulse sequences in which the **k**-space data are sampled more efficiently than with standard acquisition methods. The enhancement in the temporal resolution that can be achieved using these ultra-fast MRI methods will depend on the relaxation times of the system and correspondingly the number of echoes that can be acquired from a single excitation. For instance, typical transverse relaxation times for fluid-saturated rock core samples are in the range of several tens to hundreds of milliseconds. Therefore, considering a multi-echo MRI acquisition of a saturated rock core characterised by $T_2 = 100$ ms, with an echo time $T_E = 5$ ms, it is reasonable to suggest that 32 lines of **k**-space can be acquired from each excitation, resulting in a 32-fold enhancement in the temporal resolution compared to spin-warp, for instance. For systems that exhibit shorter relaxation times, fewer echoes can be acquired from a single excitation but significant time savings can be achieved nonetheless.

In the application to imaging of rock cores, the most commonly used ultra-fast imaging techniques are π-EPI (PEPI) [12] and RARE [13]. The latter has certain advantages over the former, in that it is both T_1- and T_2-weighted as opposed to solely T_2-weighted, which, in theory, means that the signal lifetime is longer and more echoes may be acquired from a single excitation for a given echo time [14]. Additionally, due to non-ideal radio frequency (r.f.) pulses and imperfect magnetic field gradients, PEPI is a notoriously difficult pulse sequence to implement. However, it has been shown by Xiao and Balcom [15] that by using composite broadband refocusing r.f. pulses and gradient pre-

equalization, 3D PEPI can be successfully implemented to image water saturation in rock core plugs.

It has been demonstrated that by using compressed sensing (CS), a signal with a sparse representation, such as an image, can be recovered from a number of measurements sampled below the Nyquist rate [16]. In application to the quantification of fluid content in rock cores, CS has previously been combined with pure phase-encoding techniques, due to their robustness in the presence of paramagnetic impurities and magnetic susceptibility gradients. For example, spin echo SPI (SESPI) has been used to image a water-saturated Berea sandstone core-plug: under-sampling in both phase-encoding directions, in which 20 % of a 64 × 32 **k**-space matrix was acquired, resulted in an acquisition time of 2 h [17]. Xiao and Balcom [18] have presented a method using SESPI to acquire 1D water-saturation profiles during the dynamic flooding of a sandstone rock core. It has been shown that correlations in the spatial and temporal dimensions can be exploited to enable under-sampling of **k**-*t*-space, thus resulting in significant reductions in the acquisition time. However, even with under-sampling, the pure phase encoding techniques are too slow for studying dynamic displacement processes with 3D MRI for continuous flow at representative reservoir interstial velocities.

To reduce acquisition time still further, CS can be combined with ultra-fast MRI acquisitions, thus enabling dynamic processes, such as the laboratory core flood, to be studied. A further advantage of the enhancement in temporal resolution using CS is that a higher signal-to-noise ratio (SNR) can be achieved through more signal averaging per unit acquisition time. Again, this is desirable to the petrophysics community as low-field magnets, with inherently low sensitivity, are commonly used in a core analysis laboratory. We have shown previously [19,20] that by using the RARE pulse sequence combined with CS, 3D images have been acquired in minutes as opposed to hours, as is the case with traditional acquisition techniques. In this previous work, the capability of the CS-RARE technique to observe the drainage of dodecane into a water-saturated Bentheimer sandstone core plug was demonstrated.

Previous work using MRI to investigate hydrocarbon-aqueous phase displacement core floods, has usually employed approaches to reduce the signal associated with the aqueous phase such that signal is acquired only for the hydrocarbon phase. Two methods are commonly used: (i) paramagnetic dopants (e.g. Cu^{2+}, Gd^{2+}) are used to reduce the relaxation times of the aqueous phase such that it is not detected in the image [21]: (ii) NMR-active species with comparatively low gyromagnetic ratios, such as D_2O, in the place of the H_2O-based aqueous phase, have also been employed [22]. These approaches have two drawbacks. First, since only the hydrocarbon phase is imaged, the information on the aqueous phase can only be inferred. Second, it is often desirable to characterise wettability and structure-transport characteristics of the rock using T_1-T_2 and D-T_2 measurements as part of the core analysis workflow. These measurements should be made directly on the fluids in their native state; this cannot be achieved if one of the two phases has been modified by paramagnetic doping or isotopic substitution. However,

MRI offers a further range of strategies for providing contrast between the fluid phases present which give it a particular advantage over other tomographic techniques, such as X-ray CT. The so-called non-invasive fluid contrast mechanisms that may be exploited, are: chemical selectivity of specific NMR-active nuclei detected (^{1}H, ^{13}C, ^{23}Na etc.), spectroscopic chemical shift sensitivity, longitudinal and transverse relaxation time (T_1 and T_2) weighting and diffusivity contrast. The choice of the contrast mechanism to be utilised in the imaging experiment will depend on the nature of the system under investigation and the information required. Examples of the applications of these approaches to studying rock cores are now given.

For systems in which the contributions from the hydrocarbon and aqueous phases can be resolved in the NMR spectrum, it has been shown that the chemical shift sensitivity can be used to isolate the signal from the hydrocarbon and aqueous phases independently. Dechter *et al*., [23,24] have shown that by using a pre-saturation method, fluid-specific images of refined oil and aqueous brine in carbonate (Dolomite) and sandstone (Bentheimer) cores can be obtained. This technique is expected to be particularly effective in core plug samples with a low paramagnetic content, such as certain carbonates, and less effective in clay-rich samples where chemical-shift separation is more challenging due to magnetic susceptibility gradient induced line broadening. In addition to the type of rock under investigation, the nature of the fluids within the pores must be considered to determine whether the hydrocarbon and aqueous peaks can be separated in the NMR spectrum. More specifically, the relatively complex chemical composition of crude oils is expected to result in broader peaks in the NMR spectrum than compared with alkanes, for instance, which are often used as a proxy for the hydrocarbon phase in laboratory core analysis. The magnetic field strength at which the measurements are to be made must also be considered when determining whether chemical-shift separation can be achieved for a particular fluid-rock system. This is due to the fact that as the field strength increases, the enhancement in chemical-shift sensitivity will be offset by an increase in susceptibility induced line broadening. Despite these limitations, with estimates that approximately 60 % and 40 % of the world's oil and gas, respectively, are thought to be contained in carbonate reservoirs, imaging techniques capable of studying multiphase displacements mechanisms of representative laboratory oils in such systems is considered a worthy pursuit. For cases where chemical-shift separation is not possible other contrast mechanisms are more suited, which will now be discussed.

Providing that they are sufficiently different from one another, contrast in the image may be based upon the relaxation times of the hydrocarbon and aqueous phases. One such approach is the inversion-nulling method in which species can be differentiated from one another based on their T_1 as has been demonstrated by Hall and Rajanayagam for the imaging of oil and water in sandstones [25]. Chemically-specific images of oil and water can also be obtained from T_1 or T_2 maps by integrating the signal intensity across ranges of the relaxation time spectrum and assigning to a particular fluid-phase [26]. It has also been demonstrated that ^{23}Na MRI can be used to provide independent images of the

sodium in the brine solution [27,28]. Of relevance to the present study, Washburn *et al*., [27] have demonstrated a ^{23}Na MRI method to monitor the movement of brine into an oil-saturated Bentheimer sandstone during a spontaneous imbibition process. Providing that the sodium concentration in the brine is sufficiently high to enable detection, this is perhaps the most generally applicable method across a range of rock and oil types for the measurement of only the aqueous phase within rock cores in their native state. However, one shortcoming of this method is that no direct information on the hydrocarbon phase can be obtained. Problems are also encountered, particularly when working at higher magnetic field strengths due to dissipation of the radio frequency pulses by the highly-conductive brine in the sample. Furthermore, the sensitivity of ^{23}Na nuclei relative to ^{1}H is poor, thus limiting the spatial and temporal resolution that can be achieved.

In this work, we have demonstrated the application of an MRI technique to provide high-temporal resolution, independent images of hydrocarbon and aqueous phases. By combining the CS-RARE pulse sequence with a chemically-selective preconditioning stage [23,24], 3D images of the oil and water phases have been acquired in minutes as opposed to hours, as is the case with conventional MRI techniques. Specifically, the chemically-selective CS-RARE method has been used to provide 3D images of the oil and water distributions within an Estaillades limestone core plug during a primary drainage laboratory core flood experiment.

MATERIALS AND METHODS

An Estaillades limestone core plug, 38 mm in diameter and 68 mm in length, has been used as a representative sample of a hydrocarbon-bearing reservoir rock. The rock was initially saturated with deionised water and the pore volume (P.V.) was determined by gravimetric analysis to be 22.3±0.1 ml, thus corresponding to a porosity of $\varphi = 29\pm1$ %. The sample was held in an Aflas sleeve within a PEEK rock core holder (ErgoTech, Conwy, UK), which was placed within the imaging region of the magnet. A constant confining pressure was applied to the outside of the Aflas sleeve by per-fluorinated oil (Fluorinert FC-43) using a Gilson 307 (Gilson Inc., USA) HPLC pump maintained at 250±25 psig by a back pressure regulator (Idex Health and Science, USA). Dodecane (Acros Scientific, UK), as the injectant, was pumped through the rock at a flow rate of 0.1 ml min^{-1} using a Harvard 22 syringe pump (Harvard Apparatus, USA) to mimic a primary drainage process. The MRI experiments were carried out on a 2 T (85 MHz for ^{1}H) horizontal-bore magnet controlled by a Bruker AV spectrometer. A 60 mm r.f. coil tuned to a frequency of 85.2 MHz was used for excitation and signal detection. Spatial resolution was achieved with magnetic field gradients with a maximum strength of 10.7 G cm^{-1}. In the present study, an extension of the CS-RARE method [19,20], to include a chemically-selective preconditioning section has been used. The pulse sequence diagram for the chemically-selective CS-RARE method used herein is shown in Figure 1.

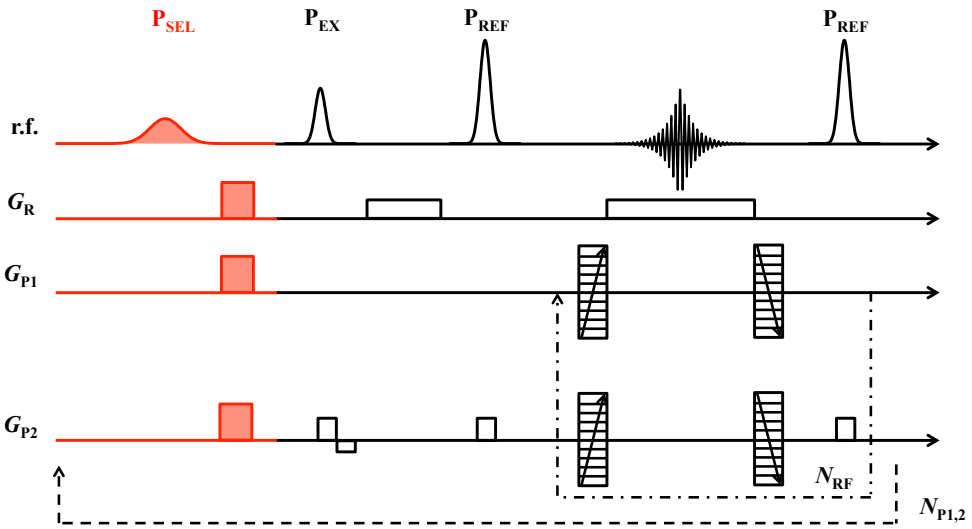

Figure 1: Schematic of the chemically-selective Rapid Acquisition with Relaxation Enhancement (RARE) pulse sequence with compressed sensing (CS). The red section represents the chemically-selective preconditioning step used to selectively excite specific regions of the NMR spectrum and the black section represents the image encoding step.

Referring to the pulse sequence diagram (Figure 1), this combines a chemically-selective preconditioning stage (red section) with the CS-RARE imaging pulse sequence (black section). For the chemically-selective excitations, Gaussian-shaped 90° excitation (P_{SEL}) pulses with a duration 4096 μs and an associated frequency bandwidth of approximately 380 Hz (width at half height), have been used. By applying P_{SEL} at an offset frequency O_{SEL}, specific regions of the NMR spectrum, corresponding to either the hydrocarbon or aqueous fluids in the rock sample, are selectively excited. Homospoil gradients (shaded boxes) in three orthogonal directions are subsequently applied for 2 ms at a strength of 5.3 G cm^{-1} to eliminate any signal associated with the spins excited by P_{SEL}. Thus the residual magnetisation available for the image acquisition is due to the spins unaffected by the P_{SEL} pulse. It follows that by applying P_{SEL} at an offset frequency of O_{SEL} = 0 Hz followed by the homospoil gradients, the signal from the water will be suppressed and an image of the dodecane within the core plug is obtained. Similarly, applying P_{SEL} at an offset frequency of O_{SEL} = -350 Hz, the signal from the dodecane will be supressed and an image of the water is obtained.

Details pertaining to the CS-RARE pulse sequence can be found in our previous publication [19,20] and the parameters specific to the work herein will now be described. Gaussian-shaped 90° excitation (P_{EX}) and 180° refocusing (P_{REF}) r.f. pulses of duration of 256 μs and power levels of 22 dB and 16 dB, respectively were used. Typical echo times for the RARE acquisitions were approximately T_E = 5 ms. The 3D images were acquired with a field-of-view (FOV) of 80 mm × 50 mm × 50 mm in the *z*, *x* and *y* directions respectively. For a data matrix size of 256 × 128 × 128 pixels in the read (*z*) direction and first (*x*) and second (*y*) phase encoding directions, this gave an image resolution of 0.31 × 0.39 × 0.39 mm pixel^{-1}. With a 25 % sampling of **k**-space, a RARE factor of

$N_{RF} = 32$ and four scans for signal averaging, the acquisition time was 17 minutes. Independent images of the dodecane and water distributions are acquired in series thus giving an acquisition time of 34 min for the total fluid saturation within the core plug sample.

RESULTS AND DISCUSSION

The results for the chemically-selective 3D MRI studies of the drainage of dodecane into a water-saturated Estaillades core plug will now be presented. Figure 2 shows a 3D image and one-dimensional profile projected along the *z*-axis of the rock prior to injection.

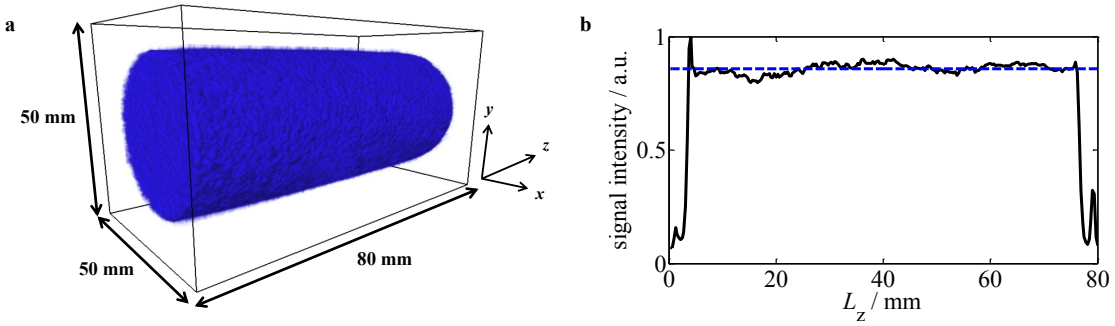

Figure 2: a) 3D image and b) one-dimensional *z*-profile of the water-saturated Estaillades core plug sample prior to the core flood. The blue dashed line in the 1D profile indicates that average saturation in the core plug. The flow in the core flood is in the *z* direction.

From this, it can be seen that core plug is uniformly saturated with water prior to the injection of dodecane. During the core flood experiment, approximately 7 P.V. of dodecane were injected into the rock and Figure 3 shows the NMR spectra acquired prior to and at the end of the core flood.

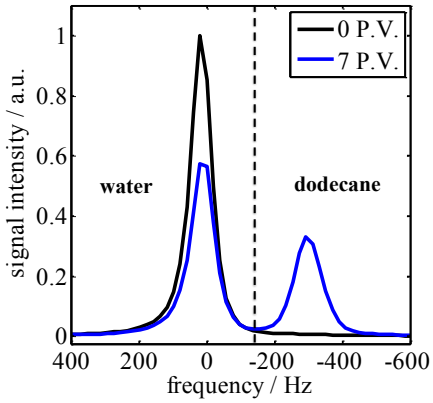

Figure 3: NMR spectra prior (0 P.V.) and following (7 P.V.) the injection of dodecane into the water-saturated Estaillades core plug sample. The signal intensity has been normalized with respect to the maximum intensity in the spectrum prior to the core flood. Signal either side of the dashed line is associated with water (left) and dodecane (right).

Prior to the core flood (0 P.V.), a contribution from only the water is seen in the NMR spectrum whereas following the injection contributions from both the water and dodecane are observed. The intensities of the water and dodecane peaks are proportional to the volume of the respective fluids within the core plug sample. By integrating the signal intensity of the NMR spectrum on either side of the cut-off (indicated by the dashed line) and correcting for the difference in hydrogen index (HI) between the water and dodecane (HI = 1.04), at the end of the core flood experiment, the water (S_w) and dodecane (S_o) saturations were determined to be $S_w = 0.62$ and $S_o = 0.38$, respectively. From Figure 3, it can be seen that the peaks in the NMR spectra assigned to the water and dodecane within the rock are resolved with very little overlap. This therefore demonstrates that this system is well-suited to this chemically-selective imaging technique.

During the core flood, chemically-selective 3D images of the dodecane and water saturation were acquired in series. For subsequent analysis, an approximately 70 mm × 14 mm × 14 mm region of interest (ROI) in the rock core has been considered. Figure 4 shows the distribution of the dodecane and water saturation within the ROI at three time points within the core flood experiment corresponding to dodecane saturations of a) $S_o = 0.06$, b) $S_o = 0.10$ and c) $S_o = 0.34$. The images on the left-hand-side (red) are of the dodecane and those on the right-hand-side (blue) are of the water.

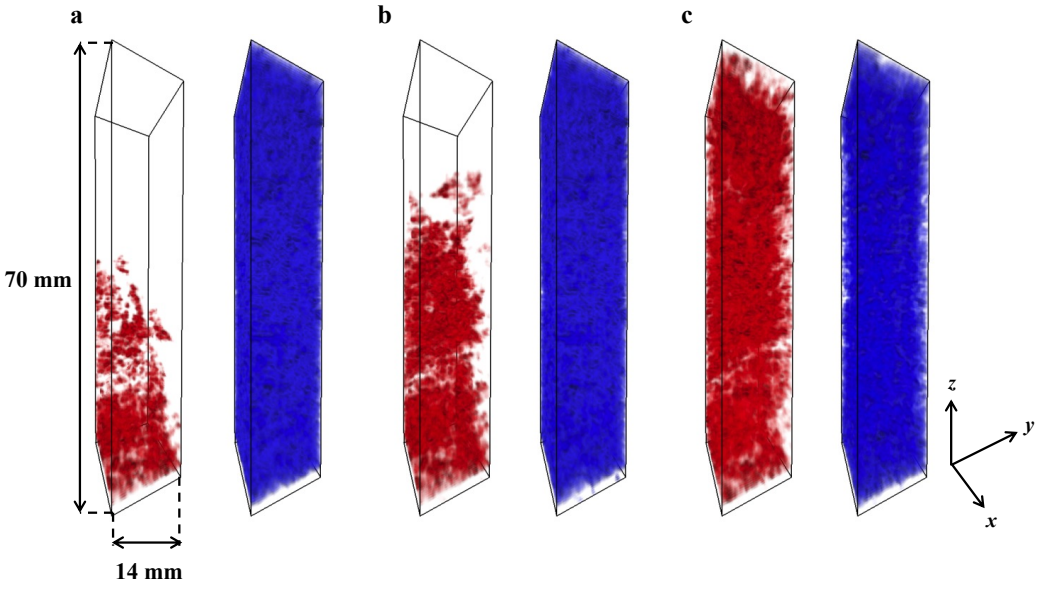

Figure 4: Chemically-selective 3D images of the dodecane (red) and water (blue) saturations within a 70 mm × 14 mm × 14 mm region of interest (ROI) at three points corresponding to dodecane saturations of a) $S_o = 0.06$, b) $S_o = 0.10$ and c) $S_o = 0.34$ at the end of the 34 min acquisition period. The flow is in the z direction.

From Figure 4, it is seen that the dodecane advances into the pore space in the form of discrete clusters before forming a more connected pathway at higher dodecane saturations. It also appears that, within the limit of the voxel resolution of the image,

water remains throughout the ROI during the displacement. As water is the wetting phase, this is to be expected as will be discussed in due course. With the flow rate of 0.1 ml min^{-1}, corresponding to an interstitial velocity of approximately 5 ft day^{-1}, 0.2 P.V. of the dodecane are injected over the period of each 34 min period for the acquisition of the dodecane and water images. For fully-sampled spin-warp and RARE images of the same acquisition parameters as the CS-RARE images presented in Figure 4, the total injected pore volumes would be 25 P.V. and 0.8 P.V., respectively. From this analysis, it is evident that the chemically-selective 3D CS-RARE technique enables a more accurate measurement of the distribution of the total fluid saturation at specific time points in the core flood and also provides the capability to investigate how the distributions of the wetting and non-wetting phases within the rock change during the displacement process.

Figure 5 shows 2D *xz* slice images of the dodecane and water saturations at two points in the core flood corresponding to dodecane saturations of $S_o = 0.06$, (a and c) $S_o = 0.10$ (b and d). The difference maps, Figure 5 e) and f), illustrate the change in saturation of the dodecane and water, respectively, between the two time points in the core flood that have been considered.

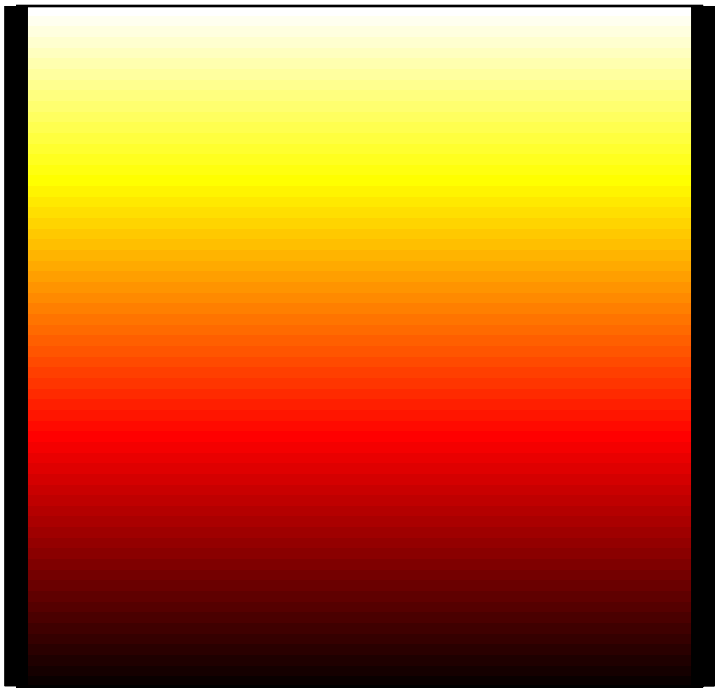

Figure 5: Chemically-selective 2D slice images (taken from the 3D images in Figure 4) in the *xz* plane for the dodecane (a and b) and water (c and d) at two time points corresponding dodecane saturations of $S_o = 0.06$ (a and c) and $S_o = 0.10$ (b and d). The corresponding difference maps between the dodecane images (a and b) and water images (c and d) are shown in e) and f), respectively.

From the images of the dodecane (Figure 5 a and b), it is clear that there is a region of the rock core whereby the local dodecane saturation remains low. This is perhaps due to the

presence of a region of relatively low permeability causing the injected dodecane to bypass and flow through higher permeability regions of the sample. This demonstrates the capability of the technique to provide insight on structure-transport relationships of the two phases within the rock core. Referring to Figure 5 c) and d), the change in saturation of the water within the rock between these two time points is much less obvious than is the case for the dodecane. This can be explained by considering the relative sizes of the pores within the rock and voxel size of the 3D image, which are on the scale of tens and hundreds of micrometres, respectively. At the pore scale, the dodecane does not displace the water completely and the residual water content will depend on various factors, such as the pore size and wettability, which in turn determine the capillary pressure that must be overcome to displace the wetting phase. Therefore, the signal intensity that is observed in each voxel is proportional to the local water saturation at that position in the rock core and is an ensemble average over many individual pores. Nevertheless, from the difference maps for the dodecane (Figure 5 e) and water (Figure 5 f), it can be seen that there is excellent agreement between the regions in which an increase in dodecane saturation and decrease in water saturation are observed. This therefore demonstrates the capability of this technique to investigate the displacement dynamics of the hydrocarbon and aqueous phases simultaneously.

CONCLUSIONS

In this paper, an MRI method to obtain independent 3D images of the hydrocarbon and aqueous fluid phases in rocks has been demonstrated for the drainage of dodecane into a water-saturated Estaillades core plug. It has been shown that the peaks in the NMR spectra that are assigned to the water and dodecane within the rock are well-resolved with very little overlap, thus demonstrating the applicability of the chemically-selective imaging technique to this system. As discussed previously, for systems in which chemical-shift separation of the oil and water cannot be achieved, other contrast mechanisms will be more suited. By using a chemically-selective preconditioning stage prior to the imaging section of the pulse sequence, independent images of water and dodecane have been acquired. From these images, it has been possible to gain insight into how the structure of rock influences the spatial distributions of the wetting and non-wetting phases during the core flood. More generally, the capability of this technique to investigate the displacement dynamics of the hydrocarbon and aqueous phases simultaneously, has been demonstrated.

The enhancement in the temporal resolution that has been achieved by using the RARE pulse sequence with CS has enabled the fluid distribution to be monitored on a time-scale that would not be possible using conventional 3D MRI protocols. The technique that has been presented herein should prove to be useful in developing the understanding of the displacement mechanisms associated with oil-water core laboratory core floods that are used for the optimisation of IOR and EOR protocols.

ACKNOWLEDGEMENTS

The authors would like to thank Royal Dutch Shell for funding this work.

REFERENCES

1. J. Mitchell, J. Staniland, A. Wilson, A. Howe, A. Clarke, E.J. Fordham, J. Edwards, R. Faber, R. Bouwmeester, Magnetic resonance imaging of chemical EOR in core to complement field pilot studies, in: International Symposium of the Society of Core Analysts, Aberdeen Scotland, UK, 27-30 August 2012: p. SCA Paper 2012–30.
2. D.D. Huang, M.M. Honarpour, Capillary end effects in coreflood calculations, in: International Symposium of the Society of Core Analysts, Montpellier, France, 8-10 September 1996: p. SCA Paper 9634.
3. P.G. Saffman, G. Taylor, The penetration of a fluid into a porous medium or Hele-Shaw cell containing a more viscous liquid, Proceedings of the Royal Society A: Mathematical, Physical and Engineering Sciences. 245 (1958) 312–329.
4. S. Davies, K.J. Packer, Pore-size distributions from nuclear magnetic resonance spin-lattice relaxation measurements of fluid-saturated porous solids. I. Theory and simulation, Journal of Applied Physics. 67 (1990) 3163-3170.
5. J. Mitchell, J. Staniland, R. Chassagne, E.J. Fordham, Quantitative in situ enhanced oil recovery monitoring using nuclear magnetic resonance, Transport in Porous Media. 94 (2012) 683–706.
6. R.L. Kleinberg, H.J. Vinegar, NMR properties of reservoir fluids, The Log Analalyst, 37 (1996) 20–32.
7. M. Fleury and F. Deflandre, Quantitative evaluation of porous media wettability using NMR relaxometry, Magnetic Resonance Imaging, 21 (2003) 385-387.
8. A.E. Pomerantz and Y-Q. Song, Quantifying spatial heterogeneity from images, New Journal of Physics. 10 (2008) 125012
9. G. Ersland, J. Husebø, A. Graue, B. A. Baldwin, J. Howard, J. Stevens, Measuring gas hydrate formation and exchange with CO_2 in Bentheim sandstone using MRI tomography, Chemical Engineering Journal. 158 (2010) 25–31.
10. K. Romanenko, D. Xiao, B.J. Balcom, Velocity field measurements in sedimentary rock cores by magnetization prepared 3D SPRITE, Journal of Magnetic Resonance, 223 (2012) 120-128.
11. W.A. Edelstein, J.M.S. Hutchison, G. Johnson, T. Redpath, Spin warp NMR imaging and applications to human whole-body imaging, Physics in Medicine and Biology. 25 (1980) 751–756.
12. P. Mansfield, Multi-planar image formation using NMR spin echoes, Journal of Physics C: Solid State Physics. 10 (1977) L55–L58.
13. J. Hennig, A. Nauerth, H. Friedburg, RARE imaging: a fast imaging method for clinical MR, Magnetic Resonance in Medicine. 3 (1986) 823–833.
14. J. Mitchell, T.C. Chandrasekera, D.J. Holland, L.F. Gladden, E.J. Fordham, Magnetic resonance imaging in laboratory petrophysical core analysis, Physics Reports. 526 (2013) 165–225.

15. D. Xiao, B.J. Balcom, π echo-planar imaging with concomitant field compensation for porous media MRI, Journal of Magnetic Resonance. 260 (2015) 38–45.
16. M. Lustig, D. Donoho, J.M. Pauly, Sparse MRI: The application of compressed sensing for rapid MR imaging, Magnetic Resonance in Medicine. 58 (2007) 1182–1195.
17. O.V. Petrov, B.J. Balcom, Two-dimensional T_2 distribution mapping in porous solids with phase encode MRI, Journal of Magnetic Resonance. 212 (2011) 102–108.
18. D. Xiao, B.J. Balcom, **k**-*t* acceleration in pure phase encode MRI to monitor dynamic flooding processes in rock core plugs, Journal of Magnetic Resonance. 243 (2014) 114–121.
19. N.P. Ramskill, I. Bush, A.J. Sederman, M.D. Mantle, L.F. Gladden, Application of Compressed Sensing MRI to Laboratory Core Floods, In Proc: International Symposium of the Society of Core Analysts, St John's, Newfoundland and Labrador, Canada, 16-21 September 2015, Society of Core Analysts. p. SCA 2015-041.
20. N.P. Ramskill, I. Bush, A.J. Sederman, M.D. Mantle, M. Benning, B.C. Anger, M. Appel, L.F. Gladden. Fast Imaging of Laboratory Core Floods using 3D RARE with Compressed Sensing, Journal of Magnetic Resonance. Submitted.
21. B.A. Baldwin, W.S. Yamanashi, NMR imaging of fluid dynamics in reservoir core, Magnetic Resonance Imaging, 6 (1988) 493–500.
22. E. Aspenes, G. Ersland, A. Graue, J. Stevens, B. A. Baldwin, Wetting phase bridges establish capillary continuity across open fractures and increase oil recovery in mixed-wet fractured chalk, Transport in Porous Media. 74 (2007) 35–47.
23. J.Dechter, R.Komoroski, S.Ramaprasad, NMR chemical shift selective imaging of individual fluids in sandstone and dolomite cores, SCA Conference - Paper Number 03, 1989.
24. J. Dechter, R. Komoroski, S. Ramaprasad, Use of presaturation for chemical-shift-selective imaging of individual fluids in sandstone and carbonate cores, Journal of Magnetic Resonance Imaging, 93 (1991) 142–150.
25. L.D. Hall, V. Rajanayagam, Thin-slice, chemical-shift imaging of oil and water in sandstone rock at 80 MHz, Journal of Magnetic Resonance. 74 (1987) 139–146.
26. D. Xiao, B.J. Balcom, Two-dimensional T_2 distribution mapping in rock core plugs with optimal **k**-space sampling, Journal of Magnetic Resonance. 220 (2012) 70–78.
27. K.E. Washburn, G. Madelin, Imaging of multiphase fluid saturation within a porous material via sodium NMR, Journal of Magnetic Resonance. 202 (2010) 122–126.
28. J. Mitchell and E.J. Fordham, Nuclear magnetic resonance core analysis at 0.3 T, Review of Scientific Instruments 85 (2014) 111502.